A multi-wavelength analysis of the cluster of galaxies ABCG 194

E. Nikogossyan[1]**, F. Durret**[2,3]**, D. Gerbal**[2,3]**, and F. Magnard**[2]

[1] Byurakan Observatory, Aragatsotn Province, 375433, Armenia
[2] Institut d'Astrophysique de Paris, CNRS, 98bis Bd Arago, F-75014 Paris, France
[3] DAEC, Observatoire de Paris, Université Paris VII, CNRS (UA 173), F-92195 Meudon Cedex, France

Abstract. We present a morphological and structural analysis of the Richness zero cluster ABCG 194, known as a "linear cluster". This study is based on a catalogue of 97 galaxies with B magnitudes and redshifts belonging to the cluster, a ROSAT PSPC image and radio data.

We show that the overall large scale structure is rather smooth and comparable at optical and X-ray wavelengths. The cluster is elongated along PA $\approx$ 50; however it appears as "linear" when taking into account only galaxies in the very central part (the axial ratio varies from 0.2 in the central region to 0.8 for a larger region). We have obtained the galaxy density profile and despite the very low X-ray emission the X-ray emitting gas density profile. We have estimated the X-ray gas and dynamical masses up to the limiting radius R_L of the PSPC image (respectively 9 10^{12} and 8 10^{13} $M_\odot$) and the stellar mass up to R_L and to 3 Mpc (3 10^{12} and 7.5 10^{12} $M_\odot$).

At smaller scales, the analysis of both positions and velocities reveals the existence of several groups but which are not strongly linked dynamically; however a main structure with a nearly gaussian velocity distribution is exhibited. The velocity dispersion is small (σ_{los} = 360 km s^{-1}). A wavelet analysis of the X-ray image reveals no large scale substructures. Small scale X-ray sources are detected, mainly corresponding to individual galaxies; we give an estimate of their luminosities. The lack of strong substructuring suggests that ABCG 194 is overall a relaxed cluster.

ABCG 194 is a poor and cold cluster; we compare how its characteristics fit into various correlations found in the literature, but generally for richer/hotter clusters, such as the σ-T_X, L_X-T_X, L_X-σ relations or the ratios of various kinds of masses.

Key words: galaxies: clusters: general – galaxies: clusters: individual: ABCG 194

1. Introduction

It is presently believed that large scale structures (in particular clusters of galaxies) are formed through hierarchical clustering. From this point of view, clusters are formed by merging of smaller clusters or by groups falling onto a larger cluster. However, the effect of merging is not the same if a cluster undergoes a major merger or accretes small groups or even single galaxies (Salvador-Solé et al. 1998).

Notice that merging does not occur isotropically around a cluster. Groups tend to fall onto clusters along filaments, thus explaining the preferential orientations often observed (see e.g. West et al. 1995, Durret et al. 1998). Therefore the true orientation and the true ellipticity are interesting quantities to derive. The imprints of such merging events can be seen directly on the X-ray images, but also in substructures which can be detected at optical (density maps, velocity structure), X-ray and radio wavelengths; this was first noticed by Baier (1977) from optical data.

Recent studies have revealed that about 50% of clusters show multi-component structure both in their galaxy distribution (Bird 1994, Escalera et al. 1994, West 1994, Maccagni et al. 1995) and in X-rays (Mohr et al. 1993, Grebenev et al. 1995, West et al. 1995, Zabludoff & Zaritsky 1995). However one may notice that, when the amount of data grows and techniques of analysis are improved, this percentage appears to grow too (Girardi et al. 1997). This leads one to question the dynamical meaning of these substructures.

The properties of relatively poor and cool clusters are somewhat more difficult to analyze because of their limited signal, but prove to be interesting as a link between rich clusters and groups. Their relaxation time scales are larger and one can wonder if they are sufficiently virialized (e.g. Mahdavi et al. 1999 and references therein). The properties of the X-ray emitting gas can be different from those of rich/hot clusters (see e.g. David et al. 1996). In particular, various relations between optical and X-ray properties (as the σ - T_X relation which seems linked to global properties), X-ray/X-ray relations (as the L_X-T_X relation) or X-ray to dynamical properties (as the X-ray gas fraction) may differ from those of rich clusters (Mahdavi et al. 1997, Markevitch 1998, Arnaud & Evrard 1999): they are probes to test cluster formation and evolution models, particularly the fine modeling of the gas heating (Cavaliere et al. 1998). Very few low temperature clusters are included in these relations, so adding even a single cluster at the border-line is important.

We present a multi-wavelength analysis of the cluster ABCG 194 based on optical data taken from the literature and on X-ray
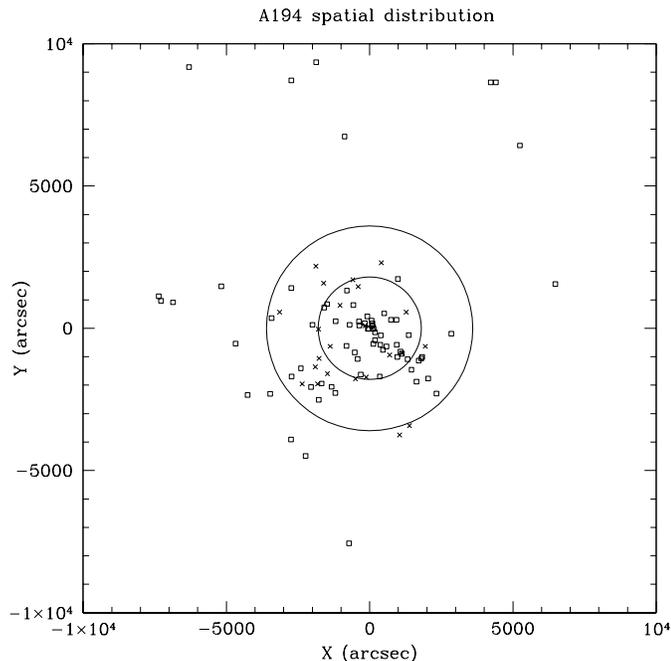

Fig. 1. Positions of the sample galaxies relative to the cluster center. Squares and crosses indicate galaxies from the CGH and BCG samples respectively. The circles have 30 arcmin and 1° radii.

Fig. 2. Digital Sky Survey image superimposed with ROSAT X-ray image contours (1, 2, 3 and 4 σ) superimposed.

data from the ROSAT archive, coupled with different techniques of analysis.

ABCG 194 is a linear cluster of richness 0 and Bautz-Morgan type III (Struble & Rood 1982) with central coordinates $\alpha_{1950} = 1^h 23.4^{mn}$ and $\delta_{1950} = -1°36'$ (Chapman et al. 1988, hereafter CGH). Its average redshift is 0.018, corresponding to a heliocentric velocity of $5340 \, \mathrm{km \, s^{-1}}$, and to a spatial scaling of 1.87 Mpc/degree ($H_0 = 50 \, \mathrm{km/s/Mpc}$, $q_0 = 0$). The velocity interval corresponding to the cluster is 4000–$6600 \, \mathrm{km \, s^{-1}}$ according to CGH, but we will show in Sect. 4.2 that it is in fact 4300–$6200 \, \mathrm{km \, s^{-1}}$.

We have somewhat arbitrarily divided our analysis into two scales: the global aspect at large scale, and the smaller scale features. The first description is related to the cluster as an astrophysical object by itself, while for the second description, which takes into account as much as possible the kinematics, dynamical processes are important.

2. The data

2.1. Optical data

Our optical analysis is based on the following data:

- Chapman et al. (1988) have observed a list of 74 cluster member galaxies in ABCG 194 (i.e. with velocities in the 4000–$6600 \, \mathrm{km \, s^{-1}}$ range), located within a radius of 3° (5.6 Mpc) around the cluster center. The CGH sample is 97% complete for galaxies brighter than B=16.7 in a region of radius R=30 arcmin around the cluster center, and 80% complete for galaxies brighter than B=15.5 in the entire region.
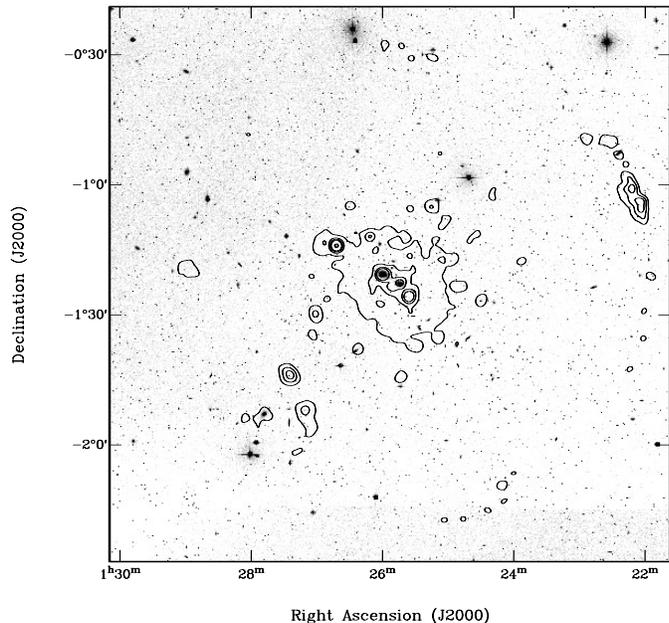
Out of the 74 galaxies in this sample, 48 and 62 are located within radii of 30 arcmin and 1° of the cluster center respectively. For all these galaxies, CGH give the following data: coordinates, radial velocity, B magnitude, morphological type, major axis position angle and ellipticity.

- We have added to this sample 22 optically fainter galaxies selected from the CF2+SSRS2 redshift survey, for which Barton et al. (1998) give positions and redshifts (hereafter the BCG sample); these authors determined that the region of 1° radius around the ABCG 194 cluster is 100% complete for galaxies brighter than $m_{Zw} = 16.46$. For the three galaxies with numbers 15, 30 and 54 in the CGH list, we take the radial velocity from the Barton et al. (1998) paper, where the error is smaller than in CGH.
- The coordinates and redshift for an additional (Seyfert) galaxy were taken from Knezek & Bregman (1998).

The total sample therefore includes 97 galaxies located within the following range of positions relative to the cluster center: $-7360 \leq X \leq 6480$ and $-7560 \leq Y \leq 8710$ arcsec.

2.2. X-ray data

Our X-ray study is based on a ROSAT PSPC image of ABCG 194 retrieved from the ROSAT data bank; the exposure time was 24482 seconds (P.I. Murray & Stephens). This image was processed with the Snowden software (Snowden et al. 1994). Obviously, this cluster is not a strong X-ray emitter, since in spite of the relatively high exposure time the total amount of counts is 8530, which is small. We show in Fig. 2 a superposition of the optical and X-ray maps, and in Fig. 3 that of the optical and radio maps. Notice that there is a zoom by a factor of $\sim$3 between these two images.
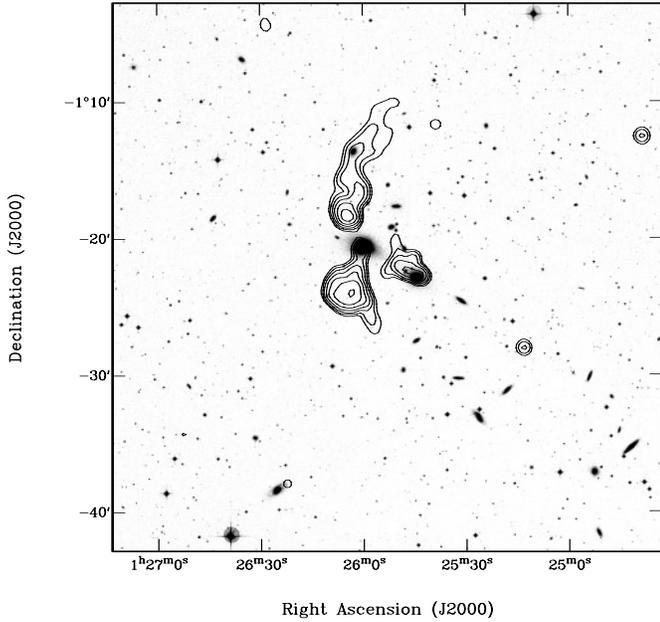
Fig. 3. Digital Sky Survey image superimposed with NVSS radio (1.4 GHz) image contours (from 12 σ up by a factor of 2).
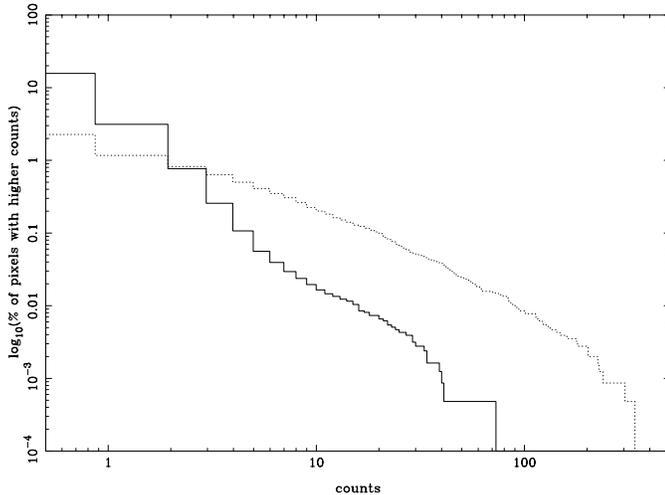

Fig. 4. Percentage of the number of pixels with a count level higher than a given value, in the weak X-ray cluster ABCG 194 (full line) and in the bright X-ray cluster ABCG 85 normalized to the same total number of counts.

In X-rays, the signal to noise ratio is low: we give in Fig. 4 the curves which allow us to obtain the number of pixels above a certain count level. 99% of the pixels contain only 1 or 2 counts (essentially noise) for both clusters; however, there are much more pixels with a large number of counts (essentially signal) in ABCG 85 than in ABCG 194.

2.3. Radio data

In the center of this cluster are located the radiosources 0123-016A and 0123-016B. The "dumbbell" source 0123-016A coincides with two galaxies, one of them being NGC 547 (3C 40),

Table 1. Equivalent radius, number of galaxies located in the disc (see text), minor to major axis ratio, direction of the major axis and center of the ellipse (in arcseconds relative to the cluster center).

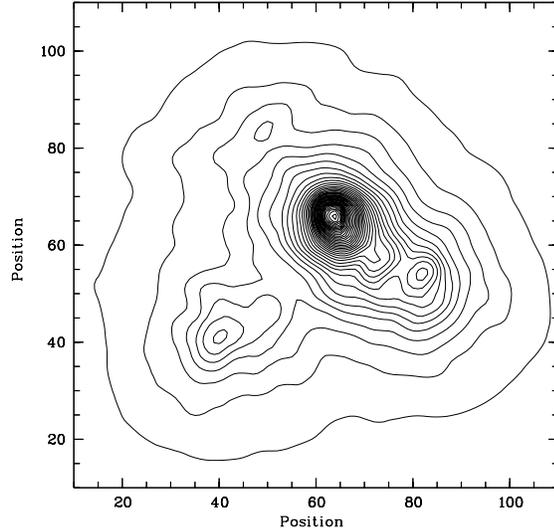|	$Disc_1$	$Disc_2$	$Disc_3$
R_{final} (arcsec)	370	1600	2860
Number of galaxies	26	42	78
b/a	0.2	0.8	0.8
Direction angle	52	45	85
Centre (X Y)	260 -218	118 -334	-272 -354

Fig. 5. Density map of the distribution of galaxies with velocities in the cluster obtained with a Dressler parameter of 10. The field size is that covered by the sample defined in Sect. 2.1., and therefore 1 pixel represents roughly 2 arcmin.

while 0123-016B coincides with NGC 541 (Ledlow & Owen 1995, Edge & Röttgering 1995); NGC 547 and NGC 541 are the first are third magnitude galaxies in the cluster respectively. The radiosource 3C 40 has a "Twin Jet" structure (Burns et al. 1994). The optical disk of NGC 547 is perpendicular to the radio axis (Zirbel & Baum 1998) and its direction coincides with that joining NGC 541 and 547 (Fasano et al. 1996). NGC 541 is a narrow-angle-tailed (NAT) radio galaxy. The direction of the tail coincides with that between NGC 541 and 547 (O'Dea & Owen 1985). According to Brodie et al. (1985) and van Breugel et al. (1985), this radio source may be interacting with Minkowski's object.

3. Morphological analysis

We present below the global morphological properties of ABCG 194 both from optical and X-ray data. After obtaining maps of the various components, we will discuss the main cluster orientations at various scales, and compare the density profiles for the galaxy distribution and for the X-ray gas.
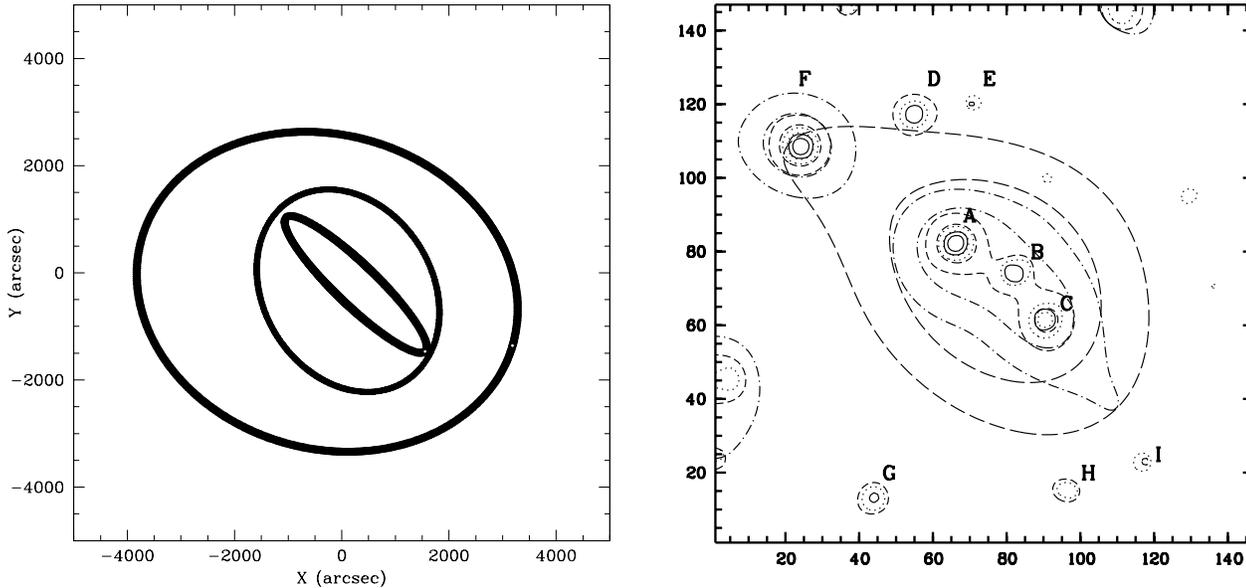
Fig. 6. Left panel **a**: Ellipse drawn as explained in the text. The corresponding equivalent radii are indicated in Table 1. Right panel **b**: Multi-scale analysis of the X-ray image showing the components at the following scales: full line: 2-pixel scale; dotted line: 4-pixel scale; dashed line: 8-pixel scale; dot-dashed line: 16-pixel scale; long dashed line: 32-pixel scale. The size of each pixel is 15×15 arcseconds. For each scale, two levels are drawn, corresponding to 3σ and 12σ of the background.

3.1. Optical analysis

The sample used in this subsection is the total one of 97 galaxies.

In order to illustrate the galaxy distribution, we have derived a Dressler map of the galaxy distribution (Dressler 1980), the main directions at various radii and the galaxy density profile.

The Dressler smoothing method has been applied to the sample of galaxies with velocities in the cluster; the result is displayed in Fig. 5. One can see that in the central part the cluster is elongated along PA$\sim$50 with a second component visible in the south east, along a direction roughly perpendicular to the main one.

We estimate these quantities with a momentum method, using the Salvador-Solé & Sanromá (1989) software: from a distribution of points in a disc of radius R_{initial}, this method gives the ellipticity and major axis direction, as well as the points which are involved in the actual ellipse (displayed in Fig. 6a), leading to an equivalent radius $R_{\mathrm{final}} = \sqrt{ab}$. The position angles and axial ratios - defined as the ratio of the small axis b to the large axis a - for the three concentric discs of radii $R \leq 1800$, $R \leq 2000$ and $R \leq 3600$ arcsec are given in Table 1. The axial ratio is seen to increase with radius, showing that despite its classification as "linear" ABCG 194 is elongated only in its central parts.

Chapman et al. (1988) have fit the ABCG 194 profile (for azimuthally averaged counts) with the following model:

$$\sigma(r) = \sigma(0)[1 + (r/r_c)^2]^{-1}$$

(resulting parameters are indicated in Table 2). The choice of this profile is questionable in comparison with a more general β-model:

$$\sigma(r) = \sigma(0)[1 + (r/r_c)^2]^{-((3\beta - 1)/2)}.$$

Table 2. Values for the β-model distribution of galaxies. Notes: (1) Chapman et al. (1988), the cluster is supposed to be spherical; (2) β fixed to 1, but the axial ratio b/a is free; (3) β and the axial ratio are both free; (4) in a rectangle of 10000^2 arcsec^2, with the b/a ratio fixed at the previous value; (5) in a rectangle of 8000^2 arcsec^2.

n_0 (N/deg^2)	β	r_c (arcsec)	b/a	Notes
150	1	720	1	(1)
330	1	518	0.8	(2)
200	1.2	1050	0.8	(3)
215	1.13	912	0.8	(4)
305	0.95	526	0.8	(5)

However, recent profile fits obtained from the ENACS data are consistent with a King model with a small dispersion on the values of β (Adami et al. 1998). C. Adami has kindly performed several fits to our data; his results are given in Table 2 (elliptical profiles are used, assuming $r = \sqrt{ab}$). It is interesting to notice that even when β is free in the fitting process (rows 3–5), its value is close to 1, in agreement with ENACS values. The axial ratio is 0.8, in agreement with the values given in Table 1.

With $\sigma_{los} = 360$ km s^{-1} and kT$_X$=2.6 keV, we can calculate β_{spec} and find a value of 0.93, consistent with the values given in Table 1.

3.2. X-ray analysis

Keeping in mind the weakness of the signal to noise ratio, we have tried to derive as much information as possible from the X-ray data.
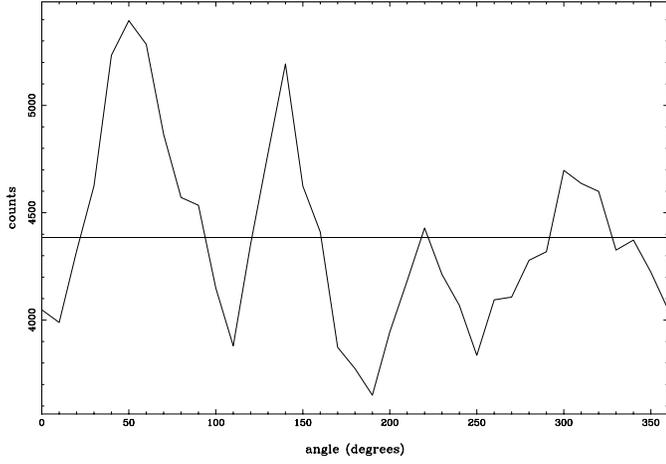
Fig. 7. Sum of counts in angular sectors $30°$ wide, with steps of $10°$. The center is that of the X-ray β-model, angle 0 is north, and angles increase counterclockwise. The image was limited to a circle of 53 arcmin radius. The number of counts per sector averaged over the whole image is shown as a straight line for comparison.
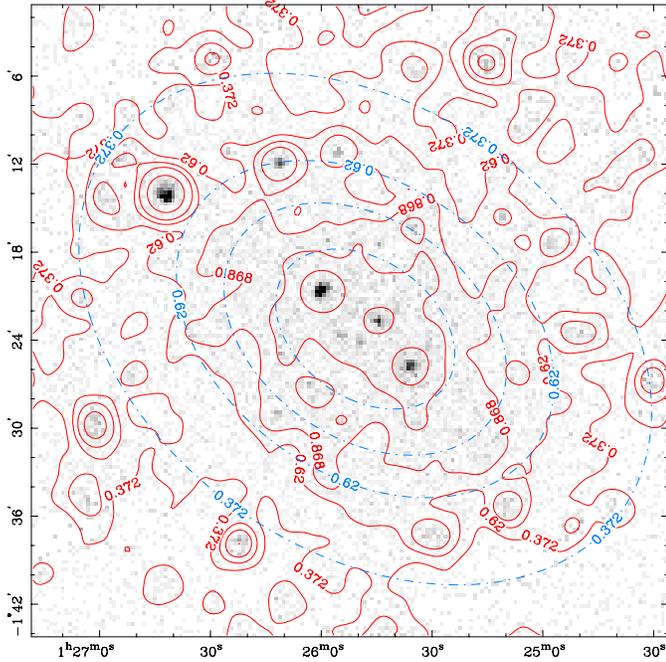

Fig. 9. 1σ, 2σ and 3σ χ^2 contours of the 1D β-model fit for the parameters $r_c - n_0$ (dotted) and $r_c - \beta$ (full line) around the values of $\chi^2_{\min}$, shown by the dashed lines.

Table 3. Results of different fits of the diffuse emission over the whole image. The sources detected by Snowden's software were not included in these fits.

Model	n_0 $(10^{-4}e^-/cm^3)$	r_c (kpc)	β	b/a	PA (°)
β model	5	524	1.02	0.7	54
King	5	515	1	0.7	54
1D β model	5	480	0.90		
1σ errors	$+1.45$ -1.1	$+646$ -185	$+1.84$ -0.27		

Fig. 8. ROSAT PSPC image (grey scale) with isocontours of the same image smoothed by a gaussian of FWHM = 7.56 pixels = 113" (full lines). The isocontours of the best pixel by pixel two dimensional β-model fit are shown as dot-dashed lines.

While two privileged directions are found from the optical analysis (see previous subsection), only one is found at first sight from the X-ray image. We have therefore made an analysis of the number of counts in angular sectors centered on the X-ray β-model center and $30°$ wide, rotating with a step of $10°$. Fig. 7 shows the existence of four peaks; the two strongest peaks correspond to PA=50 (the main principal direction of the cluster) and PA=140 pointing towards the south east optical enhancement. The third peak, which is symmetrical to that at PA=50 is

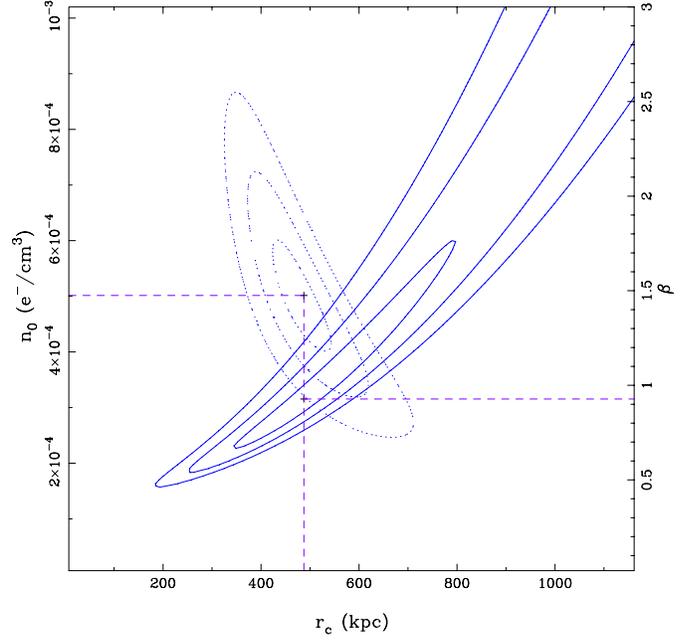very weak. The fourth peak is symmetrical to the second one, and shows that there is also X-ray emission towards the north west. Note that the first peak is certainly contaminated by the bright X-ray source labeled F in Fig. 6b.

We performed a multi scale wavelet analysis on this image to eliminate the noise and identify structures at various scales (see a full description of the method e.g. in Slezak et al. 1994). This was done in the central $35'$ diameter region (within the PSPC annulus), as illustrated in Fig. 6b. This obviously corresponds only to the central part of the cluster (see Fig. 1). The limiting radius is $R_L \simeq 1540$ arcsec, or 0.8 Mpc.

At the largest scale (32 PSPC pixels, or 4 arcmin), one can observe elliptical emission with a major axis of about $50°$ and an axial ratio $b/a \simeq 0.66$.

At a smaller scale (16 PSPC pixels, or 2 arcmin), the general behavior is similar. Due to the weight of the powerful X-ray emitting point-like source (F), the (X,Y) origin has shifted toward the west along the major axis.

The temperature was fixed to the constant value of 2.6 ± 0.15 keV measured by ASCA (Fukazawa et al. 1998).
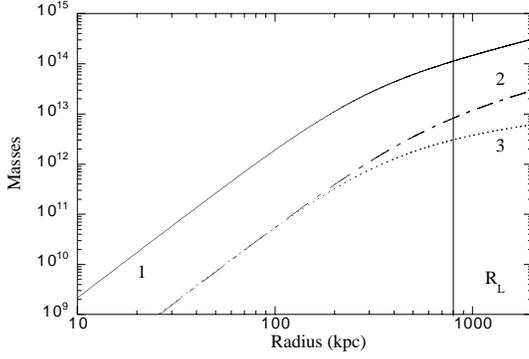
Fig. 10. Mass profiles. 1 is the dynamical mass profile assuming that the X-ray gas is isothermal; 2 - X-ray gas mass; 3 - stellar mass. Error bars on these quantities at the R_L radius are given in the text.

We calculated the bolometric X-ray luminosity by normalizing a photo-electric absorbed (galactic $n_H = 3.77\ 10^{20}\text{cm}^{-2}$) mekal model (metal abundances $= 0.3Z_\odot$, $n_e = 5\ 10^{-4}\text{cm}^{-3}$) to the source masked and background subtracted total diffuse emission (found to be 0.42 counts/sec). We find $(1.5 \pm 0.1)10^{43}$ erg s^{-1}.

We have performed a pixel by pixel fit to the data as described by Pislar et al. (1997). A β-model was used for the density law, including or not the strong point-like sources. The sources detected by Snowden's software were not included in these fits. The center is found at coordinates: $\alpha_{2000} = 1^h 25^{mn} 49^s$, $\delta_{2000} = -1°23'30''$, i.e. displaced to the south west relatively to the optical center given by CGH. The background found ($\sim$0.24 counts/pixel) is consistent with the mean background taken in an annulus far enough from the center to be flat on a wide area. Results are shown in Fig. 8: the isocontours appear rather satisfactory, but the various parameters are not well constrained (the MINOS routine from MINUIT was unable to find error boundaries). We then made a β-model fit on the profile obtained by summing the counts in elliptical bins (with their center, PA and ellipticity given by the pixel by pixel fit). This χ^2 fit leads to similar values, and to very large 1σ error bars. Fig. 9 shows how badly r_c is constrained: the 2σ contour of $\chi^2(r_c, \beta)$ stays open for very large values of r_c. The 1σ, 2σ and 3σ values are defined for $\chi^2_{red_{min}} + 1$, 4 and 9 respectively.

Note that the ellipticity found in X-rays is comparable to that in the optical (see Table 3).

3.3. Masses

The X-ray gas mass M_{gas} was calculated by integrating the β-model given in Table 3. At the limiting radius R_L=0.8 Mpc (defined as the radius where the X-ray background is reached), the X-ray gas mass is $M_{gas} = 9\ 10^{12}h_{50}^{-5/2}$ M$_\odot$, with limits corresponding to 1σ errors: $6\ 10^{12} \le M_{gas} \le 2\ 10^{13}\ h_{50}^{-5/2}$ M$_\odot$. The very large error bars are mostly due to the fact that the r_c parameter is not well constrained.

The stellar mass $M_{stellar}$ was calculated by integrating the King model given in Table 2, assuming M/L$_B$=10 M$_\odot$/L$_\odot$.

At the X-ray limiting radius R_L, the stellar mass is $(3.0 \pm 0.8)\ 10^{12}\ h_{50}^{-2}$ M$_\odot$. However, the galaxies extend much further out, up to a radius of about 3 Mpc, where the corresponding stellar mass is $(7.5 \pm 1.9)10^{12}h_{50}^{-2}$ M$_\odot$. Note that these values are not well constrained: besides the usual errors on the central density and core radius, the dominant source of error is the incompleteness of our data. In the central part of the cluster (for radii smaller than 2100 arcsec) faint galaxies are relatively more numerous than in the outskirts: 9 galaxies have magnitudes fainter than 16 while 34 are brighter than this value. The stellar luminosity inside radius R is: $L(< R) \propto n_0 R_c^3 I$, where I is the integration of the King distribution. The error on the luminosity is in fact that on $n_0 R_c^3$, which is independent of radius; the error on I is negligible. We therefore consider that the error on the stellar mass due to incompleteness at faint magnitudes is at most 25%.

The $M_{gas}/M_{stellar}$ ratio is about unity for radii smaller than $\sim$200 kpc, and reaches a value of $\sim 3 \pm 0.3$ for R_L (applying error propagation equations).

The hydrostatic equation applied to the X-ray gas allows us to estimate the total cluster dynamical mass, with hypotheses on the X-ray gas temperature. Since we have no X-ray gas temperature map, we will assume the gas to be isothermal. The corresponding mass profile is displayed in Fig. 10. The dynamical mass at radius R_L is $M_{dyn} = 8\ 10^{13}\ h_{50}^{-1}M_\odot$, with limits corresponding to 1σ errors: $3\ 10^{13} \le M_{dyn} \le 2\ 10^{14}\ h_{50}^{-1}$ M$_\odot$. Although the dynamical mass derived from the X-rays is not very accurate, it agrees with the virial mass estimated by Girardi et al. (1998).

The ratios of the X-ray and stellar masses and of the sum of these two quantities to the dynamical mass are 0.12, 0.04 and 0.16 respectively (for $h_{50} = 1$) at radius R_L. These values are only indicative within a factor of 2, due to the large error bars on the masses.

4. Structural properties

The presence of substructure in the ABCG 194 cluster of galaxies has been a subject of debate:

- Using an adaptive kernel algorithm, Kriessler & Beers (1997) determined the presence of substructure in the central core of this cluster with a probability level of 95%.

- By applying a multiscale analysis which couples kinematic estimators with wavelet transforms (Escalera et al. 1994), Girardi et al. (1997) classify the ABCG 194 cluster as unimodal with a very condensed core and two small-scale subgroups within the cluster.

- Beers & Tonry (1986) have suggested that this cluster shows good evidence for multiple X-ray substructure.

At a smaller scale - thus not really corresponding to substructures - from a $40' \times 40'$ Digital Sky Survey image around the ABCG 194 cluster center and applying a wavelet analysis technique to the corresponding ROSAT PSPC image, Lazzati et al. (1998) detected 26 X-ray sources; four of these coincide with known galaxies in the cluster: NGC 547, NGC 541, NGC 564 and NGC 538.

4.1. Optical structure

An overall description of the Dressler map has been given in Sect. 3.1. Besides the large scale morphological aspect discussed above, in particular the bright extension along PA=50 which accounts for the "linear" aspect of the cluster, we also see a fainter extension towards the south-east.

This tends to indicate the presence of substructure. In order to qualify the degree of significance of this substructure, we have applied the spatial test developed by Salvador-Solé et al. (1993), which has been shown to be well suited to the detection of substructure in systems (Scodeggio et al. 1995). By applying this method to the total sample of 97 galaxies, we estimate two density profiles: the first one, $N(r)_{dec}$, is obtained by inverting the density of numbers of pairs of galaxies, and the second one, $N(r)_{dir}$, by inverting the density of numbers of galaxies at projected distances from the center of symmetry. $N(r)_{dir}$ is therefore insensitive to correlations in galaxy positions. A difference among these two quantities is interpreted as indicating the presence of substructure in the system.

The distributions of $N(r)_{dec}$ and $N(r)_{dir}$ are displayed in Fig. 11; they are indistinguishable within error bars (estimated with a Monte Carlo technique). We have applied the statistical method proposed by Salvador-Solé et al. (1993) to test the significance of substructures at a scale chosen a priori. We find that already at a scale of 0.25 Mpc the probability to have substructure is less than 30%, and this probability strongly decreases with increasing scale. Therefore this method detects no significant substructures in the optical sample (see Salvador-Solé et al. 1993 for details). Note that the result is the same if we apply this method to a more complete magnitude limited subsample.

4.2. Substructures derived from kinematics

The previous analysis considers the cluster globally but does not take into account the dynamical properties of substructures (if any). We will therefore apply the Serna & Gerbal (1996) method, coupled with a study of the galaxy velocity distributions in the cluster.

This method sorts the galaxies according to their total energy (i.e. the sum of the potential and kinetic energies), leading to a dendogram where the total energy appears vertically. Pairs and groups of galaxies then appear with a lower total energy. The velocity density distributions were obtained using profile reconstructions based on a wavelet technique (instead of a histogram). The features obtained with this method are significant at various chosen levels above the noise (Fadda et al. 1998).

We applied this method to a sample of 97 galaxies defined as follows: the CGH velocity sample of 74 galaxies with both velocities in the cluster range and magnitudes; the BCG sample of 22 galaxies for which magnitudes were not available except for two which we found in the NED database; for the remaining 20 we assigned each galaxy the mean magnitude of the CGH sample: 15.2; one Seyfert galaxy (Knezek & Bregman 1998) to which we also assigned a magnitude of 15.2.
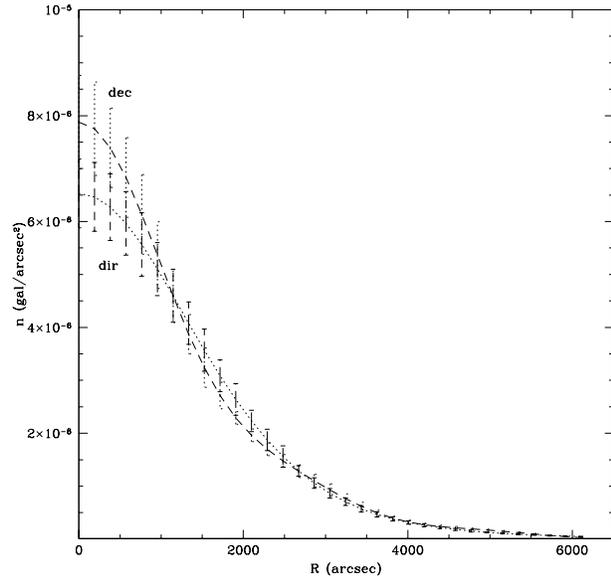

Fig. 11. $N(r)_{dec}$ and $N(r)_{dir}$ profiles (see Sect. 4.1).

A first dendogram reveals the presence of six galaxies which appear to be only very loosely linked to the cluster. The velocities of these six galaxies are quite similar, but they are distant from each other in projection on the sky. The velocity distribution indicates a bump in the $6500\,km\,s^{-1}$ region, well separated from the general distribution. We therefore chose to eliminate these objects in the following analysis, and are left with a sample of 91 galaxies; this sample leads to the velocity interval 4300–$6200\,km\,s^{-1}$ for galaxies belonging to the cluster, that is a somewhat narrower range than found by CGH. This sample will be referred to as the "All" sample, hereafter.

The velocity distribution of this new sample at various significance levels is displayed in Fig. 12a. The overall shape of this distribution is obviously not gaussian, but shows an asymmetry with an excess at high velocities. This is confirmed by the values of the skewness and kurtosis: see values for "All" in Table 4. Its mean velocity (which is also the median) is equal to that of the second brightest galaxy (NGC 541).

The dendogram obtained after excluding these six galaxies (see Fig. 12c) reveals the presence of subgroups. Groups 1 to 5 (in order of increasing mean velocity) come out of the sample easily. We have constructed a "Main" structure by taking out these five groups from the "All" sample. The statistical characteristics for these various subgroups are presented in Table 4 and a map of group positions in the overall field is shown in Fig. 13.

Group 3 appears to be the central subsystem, at the bottom of the gravitational potential well of the cluster. It contains the three brightest galaxies (including NGC 541 and NGC 547 which are both radiosources) which show a high level of boundness. Notice the presence of three other galaxies which appear to be bound together, among which the X-ray galaxy NGC 538, and also that of the Seyfert galaxy.
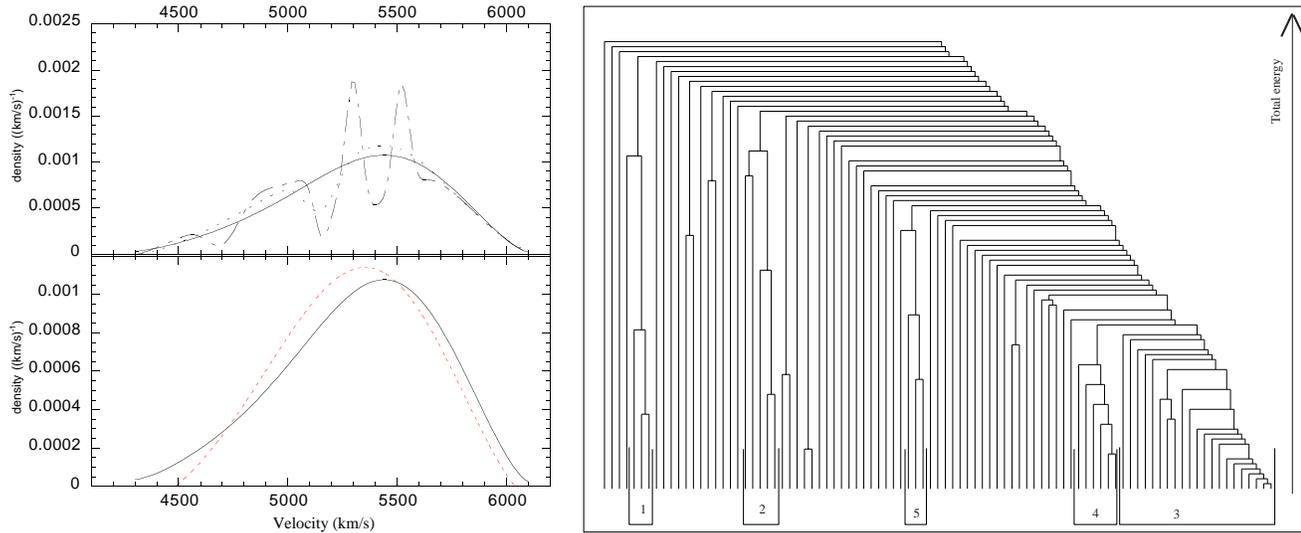
Fig. 12. Left: velocity density distribution of galaxies. Top panel **a**: galaxies belonging to the "All" sample (see text); the three densities correspond to confidence levels: 3σ (full line), 2.6σ (dotted line) and 2.2σ (dot-dashed line). Bottom panel **b**: galaxies belonging to the All (full line) and Main (dashed line) samples at a 3σ level. **c** Right: dendogram obtained by the HTree method for 91 galaxies. The numbers at the bottom correspond to those of the groups defined in Table 4.

Table 4. Characteristics of the subgroups identified from the dendogram in Fig. 12c. Columns have the following meaning: (1) group name, (2) number of members in group, (3) average radial velocity of group in $\mathrm{km\,s^{-1}}$, (4) velocity standard deviation in $\mathrm{km\,s^{-1}}$, (5) skewness, (6) kurtosis.

Name	Nb. of gal.	$\langle Vr \rangle$ ($\mathrm{km\,s^{-1}}$)	St.Dev. ($\mathrm{km\,s^{-1}}$)	Skewness	Kurtosis
All	91	5326	361	-0.37	-0.48
Group 1	5	4643	189		
Group 2	3	4805	166		
Group 3	21	5343	304	-0.07	-0.01
Group 4	6	5655	145		
Group 5	3	5895	54		
Main	53	5330	303	-0.23	-0.53

Groups 1 and 4 are well defined both spatially and in velocity space (their velocity dispersion is small). Group 4 contains the X-ray galaxy NGC 564.

Groups 2 and 5 contain only a few galaxies with small radial velocity dispersions and average intergalactic distances. Note that group 2 is far from the cluster center and appears to be weakly bound to the bulk of the cluster, as seen on the dendogram.

In comparison with the "All" sample, the "Main" structure velocity density distribution appears more gaussian, with a mean velocity equal to that of the overall sample within the error bars, but a smaller velocity dispersion and skewness (see Fig. 12b). The center of the "Main" sample is displaced towards the north east relatively to the "All" sample.

Our results can be compared to those found in the literature and based on various methods. Using a technique combining wavelets and kinematical information, Girardi et al. (1997) de-

termined the small-scale structure in the ABCG 194 cluster and found the same group as our group 2, and a group which, by coordinates and radial velocity coincides with our group 3. Using two other different methods to extract groups, Garcia (1993) also found our group 3. This group therefore appears to be at the bottom of the cluster potential well, while the other groups described in Table 4 appear more like pairs of galaxies with possible satellites.

Notice that the "linear" structure of the cluster corresponds to our group 3, while the extension observed towards the south east in the Dressler map (Fig. 5) may correspond to our group 4.

The velocity dispersion profile (VDP) is shown in Fig. 14 for the "All" sample. The binning has been performed in ellipses with their major axis along the direction PA=50 and with an axial ratio $b/a = 0.8$; the result is shown for bins of equivalent radii 400 and 800 arcsec. The shape of this profile does not change (within the error bars) if the subclusters are excluded. The VDP "inverted" shape shows an increase with radius up to ≈ 2000 arcsec, then a decrease and is comparable to that derived by den Hartog & Katgert (1996) for this cluster. These authors interpret such a profile as originating from a relaxed region.

4.3. X-ray structure

We now compare these results with the X-ray features derived first from the wavelet analysis and from the "detect" software developed by Snowden, and second from the pixel by pixel fit.

The wavelet analysis of the X-ray image reveals no substructure at middle and large scales. At the two smallest scales (2 and 4 pixels, or 30 and 60 arcsec), 9 components (at least) are detected at a 3σ level (see Fig. 6b). The Snowden method gives 38 sources in the same field, among which 9 in common with ours. The difference between the numbers of detections
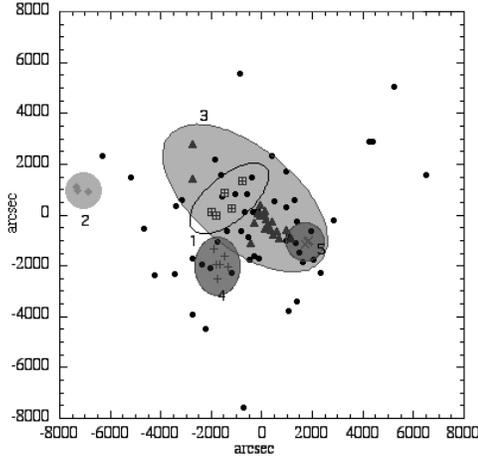
Fig. 13. Positions of subgroups in the overall cluster field. The numbers of the groups indicated correspond to those in Table 4.
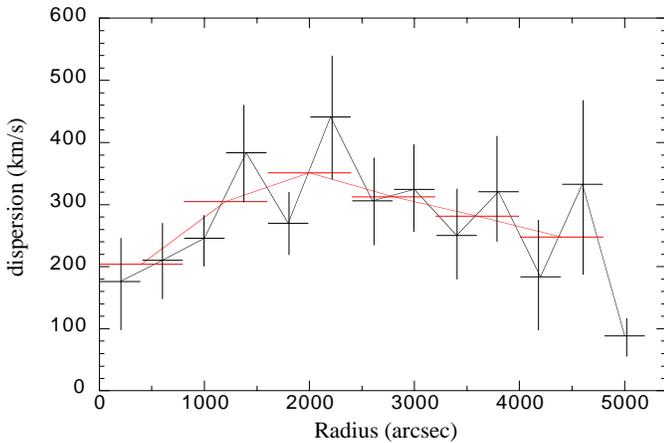

Fig. 14. Velocity dispersion as a function of radial distance to the cluster center; the equivalent radius of each bin is equal to 400 arcsec for the bold curve and to 800 arcsec for the light one.

reached by both methods raises the question of their validity. The Snowden method is based on a convolution by the PSF (which varies with radius), and is therefore close to the wavelet method. However, the statistics on which the detection thresholds are determined for both methods are not the same. Our wavelet software estimates the image characteristic statistics by analyzing the whole image (see e.g. Slezak et al. 1994) while Snowden considers only circles containing between 90% and $2.5 \times 90\%$ of the encircled energy radius of the off-axis PSF. The average background is taken into account only in the cases where there are less than 4 counts per annulus. This may explain the difference between the numbers of sources. Note also that the purpose of both methods is not the same: Snowden's software is aimed at detecting everything that is not diffuse X-ray emission, in order to eliminate these point-like sources, and therefore it tends to find a higher number of small sources (including possible cosmic rays), while our purpose is to detect only X-ray sources above a certain significance level.

Table 5. Luminosity of the sources detected in the hard band (0.44–2.04 keV). The X-ray luminosity is computed with a 1 keV mekal model.

Source	α_{2000}	δ_{2000}	counts/ksec	L_X (10^{41} erg s^{-1})
A	$1^h 26^{mn} 00^s$	$-1°20'55''$	16.8±1.1	3.1±0.2
B	$1^h 25^{mn} 45^s$	$-1°22'56''$	5.6 ±0.8	1.0±0.1
C	$1^h 25^{mn} 37^s$	$-1°26'09''$	9.6 ±0.9	1.8±0.2
D	$1^h 26^{mn} 11^s$	$-1°12'07''$	5.8 ±0.8	1.0±0.1
E	$1^h 25^{mn} 57^s$	$-1°11'18''$	2.3 ±0.5	0.4±0.1
F	$1^h 26^{mn} 43^s$	$-1°14'15''$	21.5±1.2	4.0±0.2
G	$1^h 26^{mn} 23^s$	$-1°38'11''$	3.8 ±0.6	0.7±0.1
H	$1^h 25^{mn} 31^s$	$-1°37'29''$	3.5 ±0.5	0.6±0.1
I	$1^h 25^{mn} 10^s$	$-1°35'37''$	2.6 ±0.6	0.5±0.1

Source A corresponds to one of the two "dumbbell" galaxies, which are the first and third brightest cluster galaxies; however the X-ray PSPC pixel size is too large to be able to discriminate between both galaxies. Source B can be identified with the second brightest galaxy in the cluster. Source C coincides with the Seyfert galaxy reported by Knezek & Bregman (1998). The radiosources 0123-016AB are also strong X-ray emitters (Burns et al. 1994). Note that these sources have velocities in the cluster. Source F appears to be a star (it is star-like in the POSS and there is no quasar at this position in the Véron-Cetty & Véron 1993 catalogue). The other sources do not coincide with any galaxies with available redshifts. Note that in the part of the X-ray field shown in Fig. 6b, we detect all the sources reported by Lazzatti et al. (1998) except one (their source 26).

We have estimated the X-ray luminosity of the nine detected sources, proceeding in three steps:

- we fit the whole data by a β-model as explained in Sect. 3.2;
- we subtracted to the real image the synthetic image corresponding to the values obtained by the fit;
- in the image thus obtained, we have counted the photons around the peaks corresponding to the detected sources and give the corresponding results in Table 5; we have checked that outside the sources, the background is around zero, as expected;
- the luminosities were derived from the counts assuming a temperature of 1 keV, following the method described in Sect. 3.2.

The luminosities found for these sources are much lower than those given by Lazzati et al. (1998), but the reason for such a discrepancy is not clear. We have compared our source counts with the results given by the ROSAT SASS data processing pipeline, and find that they agree within 35% except for sources B and C. Note that the specific β-model used for this estimate is not very important.

5. Conclusions

We have presented a morphological and structural analysis of ABCG 194 both at optical and X-ray wavelengths. From dynam-

ical and velocity dispersion studies, we are left with a sample of 91 galaxies really belonging to the cluster (4200–$6100\,\mathrm{km\,s^{-1}}$), the mean cluster velocity being $5326\,\mathrm{km\,s^{-1}}$ with a standard deviation of $360\,\mathrm{km\,s^{-1}}$. This value coupled with the temperature of 2.6 keV determined for this cluster from ASCA data falls on the σ-T_X relation (Wu et al. 1998). The main underlying structure (53 galaxies) has the same mean velocity but a standard deviation of $300\,\mathrm{km\,s^{-1}}$. The X-ray map shows an ellipticity similar to that observed in the optical.

The X-ray luminosity of ABCG 194 is $1.5\,10^{43}\,\mathrm{erg\,s^{-1}}$, and falls notably below the L_X-T_X relation for clusters (Markevitch et al. 1998, Arnaud & Evrard 1999), i.e. this cluster is underluminous for its temperature. On the other hand, the cluster is within the dispersion of the L_X-σ relation (Mahdavi et al. 1997). The β-model fit to the X-ray gas gives $\beta = 1.02$, which appears larger than expected from the low value of the X-ray gas temperature (Arnaud & Evrard 1999). A β-model fit to the galaxy density distribution also gives values of β consistent with 1, as in the ENACS sample (Adami et al. 1998).

ABCG 194 appears therefore to be a very poor cluster, comparable to those recently studied by Mahdavi et al. (1999), as confirmed by the stellar, X-ray gas and dynamical masses which we have calculated.

The number of counts in angular sectors from the X-ray β-model center (Fig. 7) shows privileged directions along the major axis PA found in the X-ray and optical analysis, but also along an axis perpendicular to this one. Except for individual sources, no X-ray substructures are found with a wavelet analysis. Only 9 X-ray sources are found with our method, while 38 are detected with the Snowden software.

The various analyses described above show that at large scale ABCG 194 is overall a relaxed cluster, with a few superimposed groups: the velocity distribution of the "Main" relaxed underlying cluster is not far from gaussian. However, both at optical and X-ray wavelengths, a bright linear structure is observed in the central part, and emission is much stronger south east of this line than north west. This central structure is well defined dynamically and is also rich in radio and X-ray galaxies.

We can try to interpret these results in the framework of hierarchical structure formation. As suggested by numerical simulations such as those by Tormen et al. (1997), the time interval between two possible major mergings is large compared to the timescale of violent relaxation. The cluster therefore has time to relax between two mergers. This is also the interpretation proposed for detailed features observed for example in the Coma cluster (Biviano et al. 1996). We suggest that in ABCG 194 a group around the bright elliptical galaxy NGC 547 may have merged into the cluster; due to dynamical friction, this group has stopped near the cluster center and was disrupted (González-Casado et al. 1994). The galaxy excess towards the south east could then be a remnant of this group.

ABCG 194 therefore appears as one of the very few poor clusters which are well studied at various wavelengths. Such objects are intermediate cases between rich clusters and groups, and as such are interesting to compare the physical processes taking place in these objects, which may be influenced by the very different relaxation timescales of these various systems.

References

Adami C., Mazure A., Katgert P., Biviano A., 1998, A&A 336, 63
Arnaud M., Evrard A.E., 1999, MNRAS 305, 631
Baier F.W., 1977, Astron. Nachr. 298, 151
Barton E.J., De Calvalho R.R., Geller M.J., 1998, AJ 116, 1573
Beers T.C., Tonry J.L., 1986, ApJ 300, 557
Bird C., 1994, AJ 107, 1637
Biviano A., Durret F., Gerbal D., et al., 1996, A&A 311, 95
Brodie J.P., Browyer S., McCarthy P., 1985, A&A 259,L31
Burns J.O., Rhee G., Owen F.N., Pinkney J., 1994, ApJ 423, 94
Cavaliere A., Menci N., Tozzi P., 1998, ApJ 501, 493
Chapman G.N.F., Geller M.J., Huchra J.P., 1988, AJ 95, 999
David L.P., Jones C., Forman W., 1996, ApJ 473, 692
Dressler A., 1980, ApJ 236, 351
Durret F., Forman W., Gerbal D., Jones C., Vikhlinin A., 1998, A&A 335, 41
Edge A.C., Röttgering H., 1995, MNRAS 277, 1580
Escalera E., Biviano A., Girardi M., et al., 1994, ApJ 423, 539
Fadda D., Slezak E., Bijaoui A., 1998, A&AS 127, 335
Fasano G., Falomo R., Scarpa R., 1996, MNRAS 282, 40
Fukazawa Y., Makishima K., Tamura T., et al. 1998, PASJ 50, 187
Garcia A.M., 1993, A&AS 100, 47
Girardi M., Escalera E., Fadda D., et al., 1997, ApJ 482, 41
Girardi M., Giuricin G., Mardirossian F., Mezzetti M., Boschin W., 1998, ApJ 505, 74
González-Casado G., Mamon G.A., Salvador-Solé E., 1994, ApJ 433, L61
Grebenev S.A., Forman W., Jones C., Murray S., 1995, ApJ 445, 607
den Hartog R., Katgert P., 1996, MNRAS 279, 349
Kriessler J.R., Beers T.S., 1997, AJ 113, 80
Knezek P.M., Bregman J.N., 1998, AJ 115, 1737
Lazzati D., Campana S., Rosati P., Chincarini G., Giacconi R., 1998, A&A 331, 41
Ledlow M.J., Owen F.N., 1995, AJ 109, 853
Maccagni B., Garilli M., Tarenghi M., 1995, AJ 109, 465
Mahdavi A., Böhringer H., Geller M.J., Ramella M., 1997, ApJ 483, 68
Mahdavi A., Geller M.J., Böhringer H., Kurtz M.J., Ramella M., 1999, ApJ 518, 69
Markevitch M., 1998, ApJ 504, 27
Markevitch M., Forman W.R., Sarazin C.L., Vikhlinin A., 1998, ApJ 503, 77
Mohr J.J., Fabricant D.F., Geller M.J., 1993, ApJ 413, 492
O'Dea C.P., Owen F.N., 1985, AJ 90, 927
Pislar V., Durret F., Gerbal D., Lima Neto G.B., Slezak E., 1997, A&A 322, 53
Salvador-Solé E., Sanromá M., 1989, ApJ 345, 660
Salvador-Solé E., Sanromá M., González-Casado G., 1993, ApJ 402, 398

Salvador-Solé E., Solanes J.M., Manrique A., 1998, ApJ 499, 542

Scodeggio M., Solanes J.M., Giovanelli R., Haynes M.P., 1995, ApJ 444, 41

Serna A., Gerbal D., 1996, A&A 309, 65

Slezak E., Durret F., Gerbal D., 1994, AJ 108, 1996

Snowden S.L., McCammon D., Burrows D.N., Mendenhall J.A., 1994, ApJ 424, 714

Struble M.F., Rood H.J., 1982, AJ 87, 7

Tormen G., Bouchet F.R., White S.D.M., 1997, MNRAS 286, 865

van Breugel W., Filippenko A.V., Heckman T., Miley G., 1985, ApJ 293, 83

Véron-Cetty M.-P., Véron P., 1993, A catalogue of quasars and active nuclei. 6th edition, ESO Scientific Report No. 13

West M.J., 1994, In: Durret F., Mazure A., Tran Than Van (eds.) Clusters of Galaxies. Editions Frontières

West M.J., Jones C., Forman W., 1995, ApJ 451, L5

Wu X.-P., Fang L.-Z., Xu W., 1998, A&A 338, 813

Zabludoff A.J., Zaritsky D., 1995, ApJ 447, L2

Zirbel E.L., Baum S.A., 1998, ApJS 114, 177